The 8th European Congress on Computational Methods in Applied Sciences and Engineering
ECCOMAS Congress 2022
5-–9 June 2022, Oslo, Norway

DIRECTOR-BASED IGA BEAM ELEMENTS FOR SLIDING CONTACT PROBLEMS

Paul Wasmer, Peter Betsch

Institute for Mechanics
Karlsruhe Institute of Technology
Otto-Amman-Platz 9, 76131 Karlsruhe, Germany
e-mail: paul.wasmer@kit.edu, peter.betsch@kit.edu

Key words: geometrically exact beam, sliding contact, energy-momentum scheme

Abstract. The geometrically exact beam theory is one of the most prominent non-linear beam models. It can be used to simulate aerial runways or pantograph-catenaries, where a sliding contact condition between two or more beams is used. A smooth discretization of at least C^1 continuity is needed to not introduce any unphysical kinks. This can be achieved using the isogeometric analysis, which we apply to a director-based formulation of the geometrically exact beam. For a stable time integration scheme we use an energy-momentum conserving scheme. Using the notion of the discrete gradient, an energy-momentum conserving algorithm is constructed, including the case of sliding contact between beams.

1 Introduction

The simulation of slender structures is of interest in various fields of engineering. Often Finite Element (FE) approximations with beam elements are used for this purpose. One of the most prominent beam models in the non-linear regime is the geometrically exact beam model, also known as Simo-Reissner beam. It can be viewed as a non-linear generalization of the classical linear Timoshenko beam model. Possible applications for the beam model are, for example, the simulation of aerial runways or cable cars. In this application the sliding motion of one beam along the centerline of another beam is simulated. The contact condition between the beams can hereby be modeled using a sliding joint.
Many different formulations of the geometrically exact beam model exist in the literature [4, 5, 6], mostly differing in the description of the orientation of the beam's cross-section. We use a formulation based on directors, three orthonormal vectors [8], and avoid a formulation based on rotations, as a path-independent and frame-indifferent discretization of rotations leads to additional effort in the implementation.
Balance laws for linear and angular momentum as well as the balance of energy form the bases of Hamiltonian mechanical systems, such as elastic beams. A time discretization using standard algorithms might not carry over these balance laws from the continuous to the discretized time domain. This, however, can lead to unphysical solutions or numerical instabilities, especially in the case of nonlinear configuration manifolds. As shown in many publications [14, 15], it is advantageous to employ an integration method, which preservers the structure of the continues problem in the discretization process. In [12] Gonzalez showed a general concept on the

construction of an energy-momentum conserving integrator using the so-called (G-equivariant) discrete gradient. Romero shows in [13] that the discrete gradient can be constructed from explicitly solving for Lagrange multipliers, which ensure the conserving properties. Thus, we apply an energy-momentum conserving scheme based on the discrete gradient to simulate the dynamic behavior of the beam.
In general the beam centerline can be assumed to be smooth without any kinks in a physical real-world setting. However, using a classical FE discretization with Lagrangian elements the smoothness is not preserved in the computational model, as the Lagrangian elements are C^0-continues over elements boundaries. This can be circumvented by using the concept of the Isogeometric Analysis (IGA). Initially Hughes *et al.*[1] introduced the IGA in 2005 with the goal to reduce the effort in the meshing process and close the gap between design and analysis. However, the IGA brings also more possibilities and flexibility to the Finite Element Method (FEM) in general, as well. For example the Non-Uniform Rational B-Splines (NURBS) basis functions usually employed in the IGA have the advantage that they can be easily constructed with a continuity of C^{p-1}, where p is the order of discretization. This is of great interest for the aerial runway problem as described above. Hence, we employ the IGA for the geometrically exact beam model.

In the following we give a short outline of the rest of the paper. In Section 2 we give a short summary of the beam formulation employed, as well as on the IGA concept and energy-momentum time integration scheme. In Section 3 we introduce a mixed approach to describe the sliding joint. We then use this approach to constructed a structure-preserving algorithm for the sliding joint using the G-equivariant discrete gradient.

2 Geometrically Exact Beam

Every point on the beam can be described by the position vector

$$\mathbf{x}(s,t,\theta^1,\theta^2) = \boldsymbol{\varphi}(s,t) + \boldsymbol{\theta}(s,t) = \boldsymbol{\varphi}(s,t) + \theta^\alpha \mathbf{d}_\alpha(s,t) \tag{1}$$

where $s \in [s_1, s_2]$, with $s_1, s_2 \in \mathbb{R}$, is the arc-length in the reference configuration. $\theta^i \in \mathbb{R}$ are convective coordinates (θ^1, θ^2, $\theta^3 = s$). $\boldsymbol{\varphi} \in \mathbb{R}^3$ points to the centerline of the beam and $\boldsymbol{\theta}$ gives the position on the cross-section. We employ the Einstein notation for double indices, where indices with Greek letters run from one to two ($\alpha, \beta = 1, 2$), whereas indices with Roman letters run from one to three ($i, j, k = 1, 2, 3$). Three directors $\mathbf{d}_i \in \mathbb{R}^3$ are defined, where $\mathbf{d}_1$ and $\mathbf{d}_2$ span the cross-section area of the beam, and $\mathbf{d}_3$ is defined by

$$\mathbf{d}_3(s,t) = \mathbf{d}_1(s,t) \times \mathbf{d}_2(s,t) \tag{2}$$

In the reference configuration at time $t = 0$ the director $\mathbf{d}_3(s,0)$ is equivalent to the tangent of the centerline $\mathbf{d}_3(s,0) = \boldsymbol{\varphi}_{,s}(s,0)$. Here the abbreviation of the partial derivative $\frac{\partial(\bullet)}{\partial s} = (\bullet)_{,s}$ is introduced. The directors are mutually orthonormal for all $t \in \mathbb{R}$, that is

$$\mathbf{d}_i(t) \otimes \mathbf{d}_i(t) = \mathbf{I} \tag{3}$$

where $\mathbf{I}$ is the unit tensor. The relation between the orthonormal basis $\mathbf{e}_i$ and the directors $\mathbf{d}_i$ can be expressed by

$$\mathbf{d}_i = \mathbf{R}(s,t) \cdot \mathbf{e}_i \tag{4}$$

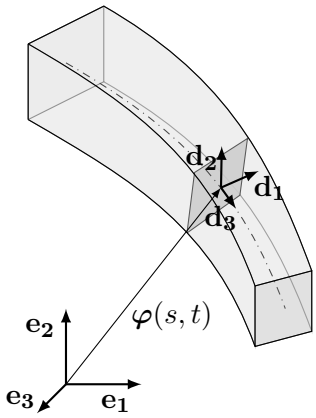

Figure 1: Sketch of the geometrically exact beam

where

$$\mathbf{R}(s,t) = \mathbf{d}_i(s,t) \otimes \mathbf{e}_i \tag{5}$$

$\mathbf{R} \in \mathrm{SO}(3)$ is an orthogonal tensor belonging to the special orthogonal group SO(3). Instead of parametrizing the orthogonal tensor $\mathbf{R}$ and discretizing the parametrization, we discretize the directors directly as proposed by Betsch and Steinmann [7, 8] and Romero [10].
The material behavior is assumed to be hyperelastic and described by the Saint Venant-Kirchhoff model. The strain measures and dynamic terms are well known in the literature and are therefore not repeated here. Extensive descriptions can be found in terms of rotations for example in [5, 6] and using directors in [7, 8, 10, 9].

2.1 Isogeometric Analysis

As mentioned in Section 1 the goal is to represent the given geometry exactly, without introducing geometrically changes due to the discretization. As mention in Sec. 1 we, thus, apply the IGA concept to the beam formulation.
The origin of NURBS basis functions lies in computer graphics. A comprehensive introduction to the topic of NURBS can be found in [2]. A NURBS curve is built from B-Splines. Each B-Spline basis is defined through a knot vector

$$\Xi_p = \big[\underbrace{0,\dots 0}_{p+1}, \underbrace{\xi_{p+2},\dots,\xi_{n_{\mathrm{ele}}+p+1}}_{n_{\mathrm{ele}}-1}, \underbrace{1,\dots 1}_{p+1}\big] \tag{6}$$

where the index p denotes the polynomial degree of the shape function and n_{ele} the number of curve segments, which is equivalent to the number of elements in a FEM sense. Eq. (6) defines an open knot vector, which is classically used in IGA.Using the knot vector a B-Spline basis can

be computed with the help of the Cox-de-Boor recursive formula [2, 3]

$$\begin{aligned} N_{i,0}(\xi) &= \begin{cases} 1 & \text{if } \xi_i \leq \xi < \xi_{i+1} \\ 0 & \text{otherwise} \end{cases} \\ N_{i,p}(\xi) &= \frac{\xi - \xi_i}{\xi_{i+p} - \xi_i} N_{i,p-1}(\xi) + \frac{\xi_{i+p+1} - \xi}{\xi_{i+p+1} - \xi_{i+1}} N_{i+1,p-1}(\xi) \end{aligned} \tag{7}$$

where division by zero is defined as zero ($\frac{(\bullet)}{0} \coloneqq 0$). The NURBS basis is constructed form

$$R_i^p(\xi) = \frac{N_{i,p}(\xi) w_i}{W(\xi)} = \frac{N_{i,p}(\xi) w_i}{\sum_{\hat{i}=1}^{n_{\text{CP}}} N_{\hat{i},p}(\xi) w_{\hat{i}}} \tag{8}$$

where w_i is the i-th weight. Introducing the control points $\mathbf{B}_i$, where $\mathbf{B}_i \in \mathbb{R}^d$ is the i-th control point, a NURBS curve can be constructed

$$\mathbf{C}(\xi) = \sum_{i=1}^{n_{\text{CP}}} R_i^p(\xi) \mathbf{B}_i \tag{9}$$

where $n_{\text{CP}} = n_{\text{ele}} + p$ is the number of control points.

The weak form is derived by applying the principle of virtual work. After applying a FE discretization a system of differential algebraic equations (DAE) is obtained

$$\mathbf{M}\,\ddot{\mathbf{q}} + \boldsymbol{\nabla} V(\mathbf{q}) + \mathbf{G_{in}}^T \boldsymbol{\lambda} = \mathbf{f}_{\text{ext}} \tag{10}$$

$$\boldsymbol{\Phi}_{\mathbf{in}}(\mathbf{q}) = \mathbf{0} \tag{11}$$

where $\mathbf{q}$ contains the values of the control points of the displacements and directors and $\boldsymbol{\lambda}$ contains the values of the Lagrange multipliers enforcing the orthonormality of the directors [8].

2.2 Time Discretization

As described in Section 1 it is of great advantage to use an energy-momentum scheme in combination with non-linear problems such as the geometrically exact beam. Using the energy-momentum scheme yields the fully discretized DAE for the geometrically exact beam

$$\mathbf{M}\mathbf{a}_{n+\frac{1}{2}} + \bar{\boldsymbol{\nabla}} V\left(\mathbf{q}_n, \mathbf{q}_{n+1}\right) + \mathbf{G}_{\text{in}}^T\left(\mathbf{q}_{n+\frac{1}{2}}\right) \boldsymbol{\lambda}_{n+1} = 0 \tag{12}$$

$$\boldsymbol{\Phi}_{\text{in}}(\mathbf{q}_{n+1}) = 0 \tag{13}$$

where

$$\mathbf{q}_{n+\frac{1}{2}} = \frac{1}{2}\left(\mathbf{q}_n + \mathbf{q}_{n+1}\right) \tag{14}$$

$$\mathbf{v}_n = \frac{2}{\Delta t}(\mathbf{q}_n - \mathbf{q}_{n-1}) - \mathbf{v}_{n-1} \tag{15}$$

$$\mathbf{a}_{n+\frac{1}{2}} = \frac{2}{\Delta t^2}\left(\mathbf{q}_{n+1} - \mathbf{q}_n\right) - \frac{2}{\Delta t}\mathbf{v}_n \tag{16}$$

Δt is the time step and $\mathbf{q}_n$ the control point values at time $n\,\Delta t$, and $\mathbf{q}_{n+1}$ the control point values at time $(n+1)\,\Delta t$ respectively (analogous for $\boldsymbol{\lambda}_{n+1}$). $\bar{\boldsymbol{\nabla}}\mathbf{f}$ is called the discrete gradient of a function $\mathbf{f}$ [12]

$$\bar{\boldsymbol{\nabla}}\mathbf{f} = \boldsymbol{\nabla}\mathbf{f}(\mathbf{q}_{n+\frac{1}{2}}) + \frac{\mathbf{f}(\mathbf{q}_{n+1}) - \mathbf{f}(\mathbf{q}_n) - \boldsymbol{\nabla}\mathbf{f}(\mathbf{q}_{n+\frac{1}{2}})\Delta\mathbf{q}}{\|\Delta\mathbf{q}\|^2}\Delta\mathbf{q} \tag{17}$$

According to Gonzalez [12] it has to fulfill the following properties to inherit the symmetry properties (linear and angular momentum and energy) from the continuous problem

- directionality condition

$$\bar{\boldsymbol{\nabla}}\mathbf{f}\left(\mathbf{q}_n, \mathbf{q}_{n+1}\right)\left(\mathbf{q}_{n+1} - \mathbf{q}_n\right) = \mathbf{f}(\mathbf{q}_{n+1}) - \mathbf{f}\left(\mathbf{q}_n\right) \tag{18}$$

- consistency condition

$$\bar{\boldsymbol{\nabla}}\mathbf{f}\left(\mathbf{q}_n, \mathbf{q}_{n+1}\right) = \bar{\boldsymbol{\nabla}}\mathbf{f}\left(\frac{\mathbf{q}_n + \mathbf{q}_{n+1}}{2}\right) + \mathcal{O}\left(\|\mathbf{q}_{n+1} - \mathbf{q}_n\|\right) \tag{19}$$

In case of a quadratic strain energy function, such as a Saint Veant-Kirchhoff material, the discrete gradient uses the average of the strains and not the average of the configurations such as with the midpoint rule [14].

2.2.1 Flying Spaghetti

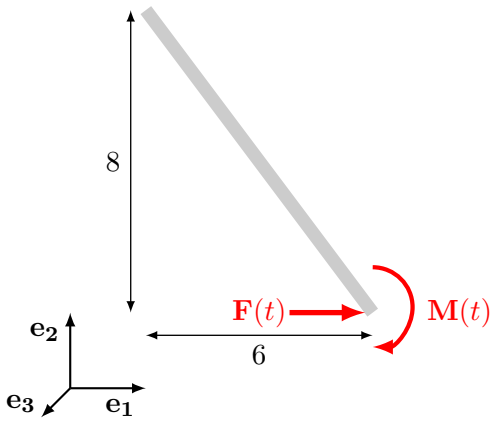

Figure 2: Sketch of the geometrically exact beam

To show the conserving properties we simulate the well known "Flying Spaghetti" example [6]. The initial geometry is shown in Fig. 2. An initially straight beam is loaded with a point force and a moment at one end. Both are given by

$$\mathbf{F}(t) = \begin{cases} 8\,\mathbf{e}_1 & \text{for} \quad t \leq 2.5 \\ \mathbf{0} & \text{else} \end{cases} \qquad \mathbf{M}(t) = \begin{cases} -80\,\mathbf{e}_3 & \text{for} \quad t \leq 2.5 \\ \mathbf{0} & \text{else} \end{cases}$$

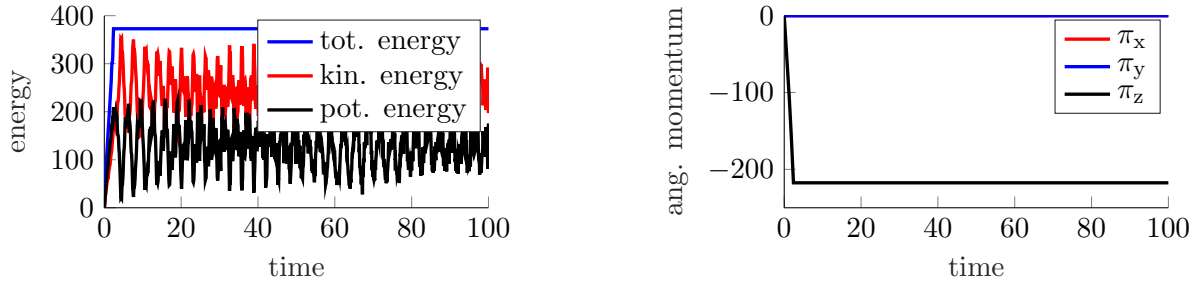

(a) Energy over time

(b) Angular momentum over time

Figure 3: Simulation results of the Flying Spaghetti

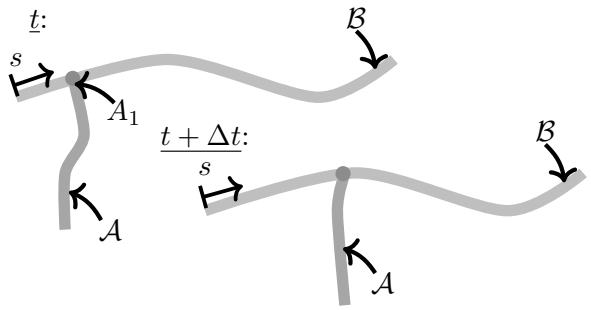

Figure 4: Sketch of the sliding beam problem

The beam parameters are given by

$$GA = 10.000 \qquad EA = 10.000 \qquad A_\rho = 1$$
$$EI = 100 \qquad GJ = 200 \qquad M_\rho = 10$$

The evolution of the energy and angular momentum are displayed in Fig. 3, where a constant time step of $\Delta t = 0.1$ was used. It can be seen that both quantities are constant over the whole simulation time after $t = 2.5$, from which on no external loads are present anymore.

3 Sliding Joint

For the sliding beam problem, we assume that two beams are in contact, where one beam is moving along the centerline of the other for a given fixed point. A sketch of the problem is shown in Fig. 4. For convenience we here chose the end, point A_1, of beam $\mathcal{A}$. Due to the collocation properties of the open knot vectors, this simplifies the implementation. However, a generalization can be performed in an analogous way. The goal is to simulate the sliding without any unphysical kinks, which might arise due to the chosen discretization. Hence, the discretization order has to be choosen of order higher than one ($p > 1$).

Here beam $\mathcal{A}$ slides along the centerline of beam $\mathcal{B}$, while always staying in contact at point A_1. Both beams are modeled as geometrically exact beams and can deform. A detailed sketch of the contact is shown in Fig. 5.

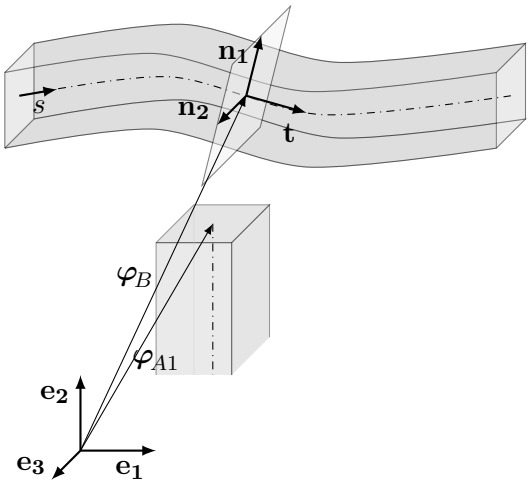

Figure 5: Detailed sketch of the contact problem

The described contact problem is similar two a Node-to-Segment (NTS) algorithm, known from contact mechanics. The construction of the structure conserving algorithm thus follows closely the NTS algorithm of [16].
The contact constraints can be formulated as

$$\mathbf{\Phi}_{\mathrm{c}} = \begin{bmatrix} (\boldsymbol{\varphi}_{A1} - \boldsymbol{\varphi}_B(s_{\mathrm{c}})) \cdot \mathbf{n}_1 \\ (\boldsymbol{\varphi}_{A1} - \boldsymbol{\varphi}_B(s_{\mathrm{c}})) \cdot \mathbf{n}_2 \end{bmatrix} \tag{20}$$

where the normal vectors can be calculated using the Sernet-Fernet frame

$$\mathbf{t} = \frac{\boldsymbol{\varphi}_{B,s}\left(s_{\mathrm{c}}\right)}{\left\|\boldsymbol{\varphi}_{B,s}\left(s_{\mathrm{c}}\right)\right\|} \tag{21}$$

$$\mathbf{n}_1 = \frac{\boldsymbol{\varphi}_{B,ss}\left(s_{\mathrm{c}}\right)}{\left\|\boldsymbol{\varphi}_{B,ss}\left(s_{\mathrm{c}}\right)\right\|} \tag{22}$$

$$\mathbf{n}_2 = \mathbf{t} \times \mathbf{n}_1 \tag{23}$$

$\boldsymbol{\varphi}_{A1}$ is the position vector of point A_1. s_{c} is the arc-length of beam $\mathcal{B}$ at the contact point. Thus, $\boldsymbol{\varphi}_B$ is the position of the centerline of $\mathcal{B}$, where the contact occurs. The mutually orthonormal vectors $\mathbf{n}_1$ and $\mathbf{n}_2$ span the plane perpendicular to the tangent of the centerline at the arc-length s_{c}.

3.1 Mixed approach

We here introduce s_{c} as well as $\mathbf{n}_1$ and $\mathbf{n}_2$ as augmented coordinates [17]

$$\hat{\mathbf{q}} = \begin{bmatrix} s_{\mathrm{c}} \\ \mathbf{n}_1 \\ \mathbf{n}_2 \end{bmatrix} \tag{24}$$

The normal vectors $\mathbf{n}_1$ and $\mathbf{n}_2$ are equivalent to normal vectors in Eq. (20), hence no additional subscripts are introduced. The augmented coordinates are appended to the global coordinate

vector

$$\bar{\mathbf{q}} = \begin{bmatrix} \mathbf{q} \\ \hat{\mathbf{q}} \end{bmatrix} \tag{25}$$

With the augmented coordinates arise additional constraints confining the augmented coordinates

$$\boldsymbol{\Phi}_{\mathrm{a}} = \begin{bmatrix} (\boldsymbol{\varphi}_{A1} - \boldsymbol{\varphi}_B(s_{\mathrm{c}})) \cdot \boldsymbol{\varphi}_{B,s}(s_{\mathrm{c}}) \\ \mathbf{n}_1 \cdot \mathbf{n}_1 - 1 \\ \mathbf{n}_2 \cdot \mathbf{n}_2 - 1 \\ \mathbf{n}_1 \cdot \mathbf{n}_2 \\ \mathbf{n}_1 \cdot \boldsymbol{\varphi}_{B,s}(s_{\mathrm{c}}) \\ \mathbf{n}_2 \cdot \boldsymbol{\varphi}_{B,s}(s_{\mathrm{c}}) \\ \mathbf{n}_1 \cdot \left(\boldsymbol{\varphi}_{A1} - \boldsymbol{\varphi}_B^{a+p} \right) \end{bmatrix} \tag{26}$$

The superscript a depends on the element (or knot span) on which the contact occurs on beam $\mathcal{B}$. $\boldsymbol{\varphi}_B^{a+p}$ is position of the $a+p$-th control point. The first constraint $\Phi_{\mathrm{a},1}$ determines the augmented coordinate s_{c}. The constraints $\Phi_{\mathrm{a},2}$ through $\Phi_{\mathrm{a},4}$ ensure that the vectors $\mathbf{n}_1$ and $\mathbf{n}_2$ are orthonormal. Similarly, $\Phi_{\mathrm{a},5}$ and $\Phi_{\mathrm{a},6}$ enforce that tangent vector $\boldsymbol{\varphi}_{B,s}(s_{\mathrm{c}})$ is orthogonal to the plane spanned by $\mathbf{n}_1$ and $\mathbf{n}_2$. $\Phi_{\mathrm{a},7}$ hinders the rotation of $\mathbf{n}_1$ and $\mathbf{n}_2$ around $\boldsymbol{\varphi}_{B,s}(s_{\mathrm{c}})$.
The contact constraints and the constraints of the augmented coordinates are collected in the constraint vector

$$\mathbf{g}(\bar{\mathbf{q}}) = \begin{bmatrix} \bar{\boldsymbol{\Phi}}_{\mathrm{c}}(\bar{\mathbf{q}}) \\ \boldsymbol{\Phi}_{\mathrm{a}}(\bar{\mathbf{q}}) \end{bmatrix} \tag{27}$$

3.2 G-equivarient discrete gradient

According to Gonzalez [12] the discrete G-equivarient gradient for a function $\mathbf{f}$ is given by

$$\bar{\boldsymbol{\nabla}}^G \mathbf{f} = \boldsymbol{\nabla}_q \boldsymbol{\pi} \bar{\boldsymbol{\nabla}}_\pi \bar{\mathbf{f}} \tag{28}$$

where $\bar{\boldsymbol{\nabla}}_\pi \bar{\mathbf{f}}$ is the discrete gradient given by (17). The discrete G-equivarient discrete gradient fulfills two conditions

- equivariance condition

$$\bar{\boldsymbol{\nabla}}^G \mathbf{f}(\Phi_g(\mathbf{q}_{n+1}), \Phi_g(\mathbf{q}_n)) = \left(\boldsymbol{\nabla} \Phi_g \left(\mathbf{q}_{n+\frac{1}{2}} \right) \right)^{-T} \cdot \bar{\boldsymbol{\nabla}}^G \mathbf{f} \left(\mathbf{q}_{n+1}, \mathbf{q}_n \right) \tag{29}$$

- orthogonality condition

$$\bar{\boldsymbol{\nabla}}^G \mathbf{f} \left(\mathbf{q}_{n+1}, \mathbf{q}_n \right) \cdot \boldsymbol{\xi}_p \left(\mathbf{q}_{n+\frac{1}{2}} \right) = 0 \tag{30}$$

$\boldsymbol{\pi}$ is a set of (quadratic) invariants. They can be found according to Cauchy's representation theorem [4]. The formulation of the invariants is dependent on the chosen discretization order, which, as mentioned above, has to be greater than one. We show here the formulation for a discretization order of $p = 2$. Formulation for higher orders follow in a similar fashion. The

vector of invariants is given by

$$\boldsymbol{\pi} = \begin{bmatrix} s_{\mathrm{c}} \\ \mathbf{n}_1^T \mathbf{n}_1 \\ \mathbf{n}_2^T \mathbf{n}_2 \\ \mathbf{n}_1^T \mathbf{n}_2 \\ \left(\boldsymbol{\varphi}_{A1} - \boldsymbol{\varphi}_B^{a+2}\right)^T \mathbf{n}_1 \\ \left(\boldsymbol{\varphi}_{A1} - \boldsymbol{\varphi}_B^{a}\right)^T \mathbf{n}_1 \\ \left(\boldsymbol{\varphi}_B^{a+1} - \boldsymbol{\varphi}_B^{a}\right)^T \mathbf{n}_1 \\ \left(\boldsymbol{\varphi}_B^{a+2} - \boldsymbol{\varphi}_B^{a}\right)^T \mathbf{n}_1 \\ \left(\boldsymbol{\varphi}_{A1} - \boldsymbol{\varphi}_B^{a}\right)^T \mathbf{n}_2 \\ \left(\boldsymbol{\varphi}_B^{a+1} - \boldsymbol{\varphi}_B^{a}\right)^T \mathbf{n}_2 \\ \left(\boldsymbol{\varphi}_B^{a+2} - \boldsymbol{\varphi}_B^{a}\right)^T \mathbf{n}_2 \\ \left(\boldsymbol{\varphi}_B^{a+1} - \boldsymbol{\varphi}_B^{a}\right)^T \left(\boldsymbol{\varphi}_{A1} - \boldsymbol{\varphi}_B^{a}\right) \\ \left(\boldsymbol{\varphi}_B^{a+2} - \boldsymbol{\varphi}_B^{a}\right)^T \left(\boldsymbol{\varphi}_{A1} - \boldsymbol{\varphi}_B^{a}\right) \\ \left(\boldsymbol{\varphi}_B^{a+1} - \boldsymbol{\varphi}_B^{a}\right)^T \left(\boldsymbol{\varphi}_B^{a+1} - \boldsymbol{\varphi}_B^{a}\right) \\ \left(\boldsymbol{\varphi}_B^{a+2} - \boldsymbol{\varphi}_B^{a}\right)^T \left(\boldsymbol{\varphi}_B^{a+1} - \boldsymbol{\varphi}_B^{a}\right) \\ \left(\boldsymbol{\varphi}_B^{a+2} - \boldsymbol{\varphi}_B^{a}\right)^T \left(\boldsymbol{\varphi}_B^{a+2} - \boldsymbol{\varphi}_B^{a}\right) \end{bmatrix} \tag{31}$$

We introduce the following abbreviations

$$\bar{\mathbf{N}} = \begin{bmatrix} N_{a+1}(\pi_1) & N_{a+2}(\pi_1) \end{bmatrix}^T \tag{32}$$

$$\bar{\mathbf{N}}_{,\pi_1} = \begin{bmatrix} N_{a+1\,,\pi_1}(\pi_1) & N_{a+2\,,\pi_1}(\pi_1) \end{bmatrix}^T \tag{33}$$

$$\hat{\boldsymbol{\pi}} = \begin{bmatrix} \pi_7 & \pi_8 \end{bmatrix}^T \tag{34}$$

$$\tilde{\boldsymbol{\pi}} = \begin{bmatrix} \pi_{10} & \pi_{11} \end{bmatrix}^T \tag{35}$$

$$\mathring{\boldsymbol{\pi}} = \begin{bmatrix} \pi_{12} & \pi_{13} \end{bmatrix}^T \tag{36}$$

$$\bar{\boldsymbol{\pi}} = \begin{bmatrix} \pi_{14} & \pi_{15} \end{bmatrix}^T \tag{37}$$

$$\overset{*}{\boldsymbol{\pi}} = \begin{bmatrix} \pi_{15} & \pi_{16} \end{bmatrix}^T \tag{38}$$

With the help of Eq. (32) - (38) the constraints are rewritten in a compact manner

$$\bar{\mathbf{g}}(\boldsymbol{\pi}) = \begin{bmatrix} \pi_6 - \bar{\mathbf{N}}^T \hat{\boldsymbol{\pi}} \\ \pi_9 - \bar{\mathbf{N}}^T \tilde{\boldsymbol{\pi}} \\ \bar{\mathbf{N}}_{,\pi_1}^T \mathring{\boldsymbol{\pi}} - N_2(\pi_1) \bar{\mathbf{N}}_{\pi_1}^T \bar{\boldsymbol{\pi}} - N_3(\pi_1) \bar{\mathbf{N}}_{\pi_1}^T \overset{*}{\boldsymbol{\pi}} \\ \pi_2 - 1 \\ \pi_3 - 1 \\ \pi_4 \\ \bar{\mathbf{N}}_{,\pi_1}^T \hat{\boldsymbol{\pi}} \\ \bar{\mathbf{N}}_{,\pi_1}^T \tilde{\boldsymbol{\pi}} \\ \pi_5 \end{bmatrix} \tag{39}$$

The reformulation can be achieved by using the partition of unity of the shape functions. The contact constraints than lead to the following set of DAE's

$$\begin{aligned} \mathbf{M}\mathbf{a}_{n+\frac{1}{2}} + \bar{\boldsymbol{\nabla}} V(\mathbf{q}_{n+1}, \mathbf{q}_n) + \mathbf{G}_{\text{in}}^T(\mathbf{q}_{n+\frac{1}{2}})\boldsymbol{\lambda}_{n+1} + \bar{\boldsymbol{\nabla}}^G \bar{\mathbf{g}}(\boldsymbol{\pi}_{n+1}\left(\bar{\mathbf{q}}_{n+1}\right), \boldsymbol{\pi}_n(\bar{\mathbf{q}}_n)\right)\boldsymbol{\lambda}_{\text{c},n+1} &= 0 \\ \boldsymbol{\Phi}_{\text{in}}(\mathbf{q}_{n+1}) &= 0 \\ \bar{\mathbf{g}}(\boldsymbol{\pi}_{n+1}(\bar{\mathbf{q}}_{n+1})) &= 0 \end{aligned} \tag{40}$$

3.2.1 Rotating beam

As a verification example we simulate two beams. They can move freely except for the sliding contact constraint between them. The initial configuration is shown in Fig. 6. The beams have the following initial velocities

$$\mathbf{v}_0 = \begin{bmatrix} 1 & 8\,z & 0 \end{bmatrix}^T \qquad \mathbf{v} = \begin{bmatrix} 0 & 0 & 1 \end{bmatrix}^T$$

as well as an angular velocity distribution

$$\boldsymbol{\omega}_0 = \begin{bmatrix} 2 & 0 & 0 \end{bmatrix}^T$$

as shown in Fig. 6a. The beam parameters are given by

$$\begin{aligned} GA &= 5.000 & EA &= 10.000 & A_\rho &= 1 \\ EI &= 10 & GJ &= 10 & M_\rho &= 1 \cdot 10^{-3} \end{aligned}$$

The simulation results for the energy and the angular momentum are shown in Fig. 6, where a time step of $\Delta t = 0.0275$ is used. In Fig. 6b the total energy of both beams is shown for two different time stepping schemes, the energy-momentum method (EM), developed above and the classical midpoint rule. As can be clearly seen, the midpoint rule leads to an energy blow up, whereas the proposed EM method conserves the energy. In Fig. 6c the angular momentum results of the EM scheme of the total system are shown. It can be seen that all components are conserved.

4 Summary and outlook

We employed the well-known isogeometric concept to the geometrically exact beam formulation. Instead of describing the cross-section orientation of the beam with rotation variables, directors were used. This was done to simulate a sliding spherical joint between two beams with the goal to construct an energy-momentum conserving algorithm. The contact condition was described using augmented coordinates enabling the construction of a vector of invariants, which is needed for the construction of the discrete gradient.
The applied formulation with directors leads to an increase in unknowns. It would be, hence, of great interest to investigate different descriptions. An interesting concept could be unit quaternions to describe the orientation of the cross-section [11].
To circumvent the additional constraints of the contact condition, the discrete null space method can be applied [18].

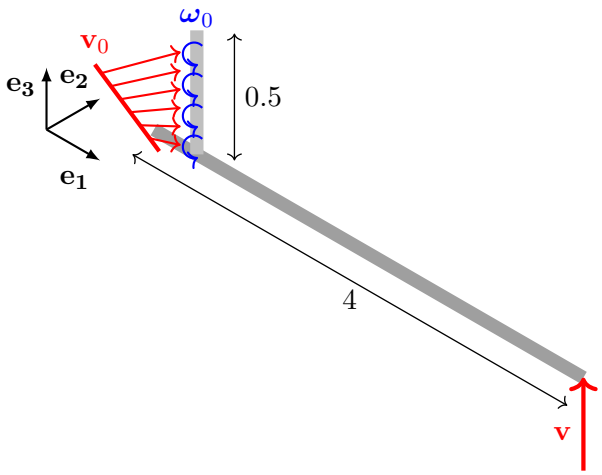

(a) Sketch of the rotating beam

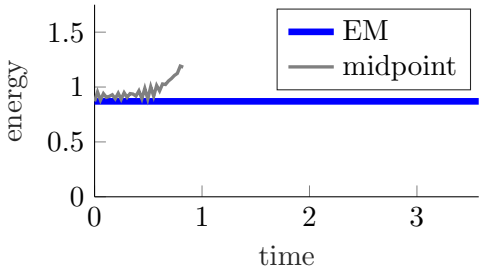

(b) Total energy of the system over time

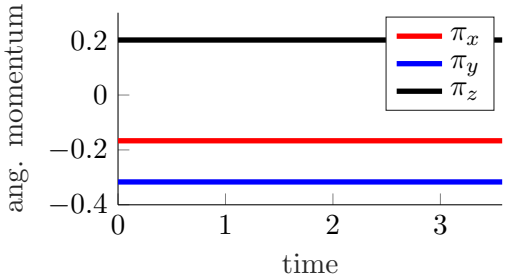

(c) Angular momentum over time

Figure 6: Simulation results of the rotating beam

REFERENCES

[1] Hughes, T.J.R., Cottrell, J.A., Bazilevs Y., Isogeometric analysis: CAD, finite elements, NURBS, exact geometry and mesh refinement, *Comput Method Appl M* (2005) **194**,39: 4135-4195.

[2] Piegl, L. and Tiller, W., *The NURBS Book*. Springer-Verlag Berlin Heidelberg GmbH, (1997).

[3] Cottrell, J.A., Hughes, T.J.R., Bazilevs, Y. *Isogeometric Analysis - Toward Integration of CAD and FEA*. John Wiley and Sons, Ltd., (2009).

[4] Antmann, S.S. *Nonlinear Problems of Elasticity*. Springer-Verlag New York, (2005).

[5] Simo, J.C., A finite strain beam formulation. The three-dimensional dynamic problem. Part I, *Comput Method Appl M* (1985) **49**,1: 55-70.

[6] Simo, J.C., Vu-Quoc, L., On the dynamics of flexible beams under large overall motions - the plane case: Part II *J Appl Mech*, (1986) **53**,1:855-863

[7] Betsch, P., Steinmann, P., Frame-indifferent beam finite elements based upon the geometrically exact beam theory, *Int J Numer Meth Eng* (2002) **54**,12: 1775-1788.

[8] Betsch, P., Steinmann, P., Constrained dynamics of geometrically exact beams, *Comput Mech* (2003) **31**: 49-59.

[9] Harsch, J., Capobianco, G., Eugster, S.R., Finite element formulations for constrained spatial nonlinear beam theories, *Math Mech Solids* (2021) **26**,12: 1838-1863.

[10] Romero, I., Armero, F., An objective finite element approximation of the kinematics of geometrically exact rods and its use in the formulation of an energy-momentum conserving scheme in dynamics, *Int J Numer Meth Eng* (2002) **12**: 1683-1716.

[11] Romero, I., The interpolation of rotations and its application to finite element models of geometrically exact rods, *Comput Mech* (2004) **34**: 121–133.

[12] Gonzalez, O. Time Integration and Discrete Hamiltonian Systems. *J Nonlinear Sci* (1996) **6**,5: 449-467.

[13] Romero, I. An analysis of the stress formula for energy-momentum methods in nonlinear elastodynamics, *Comput Mech* (2012) **50**: 603-610.

[14] Simo, J.C., Tarnow, N., The discrete energy-momentum method. Conserving algorithms for nonlinear elastodynamics, *ZAMM-Z Angew Math Me* (1992) **43**,2: 757-792.

[15] Simo, J. C. and Tarnow, N. and Doblare, M., Non-linear dynamics of three-dimensional rods: Exact energy and momentum conserving algorithms, *Int J Numer Meth Eng* (2005)**38**,9: 1431-1473.

[16] Hesch, C. and Betsch, P. Transient 3d contact problems—NTS method: mixed methods and conserving integration, *Comput Mech*,(2011) **48**, 437–449.

[17] Betsch, P. and Uhlar, S. Energy-momentum conversing integration of multibody dynamics, *Multibody Syst Dyn* (2007) **17**, 243-289.

[18] Betsch, P., The discrete null space method for the energy consistent integration of constrained mechanical systems. Part I: Holonomic constraints, *Comput Method Appl M* (2005) **194**,50-52,: 5159-5190.